Functional and structural characterization of allosteric activation of Phospholipase Cε by Rap1A

Monita Sieng[†#], Arielle F. Selvia[†], Elisabeth E. Garland-Kuntz[†], Jesse B. Hopkins[‡], Isaac J. Fisher[†], Andrea T. Marti[†, ‡], and Angeline M. Lyon[†§]*

[†]Department of Chemistry and [§]Department of Biological Sciences, Purdue University, West Lafayette, Indiana 47907, United States [1]and the [‡]Biophysics Collaborative Access Team, Illinois Institute of Technology, Sector 18ID, Advanced Photon Source, Argonne National Laboratory, Lemont, IL 60439

Present Addresses: [#]Sequlite Genomics, 6773 Sierra Ct, Dublin, CA 94568

*Corresponding author: Angeline M. Lyon

Email: lyonam@purdue.edu

Running title: Allosteric activation of PLCε

Keywords: calcium, intracellular release, cardiovascular disease, cell signaling, G protein, phosphatidylinositol signaling, phospholipase C, Ras-related protein 1 (Rap1), small angle X-ray scattering

ABSTRACT

Phospholipase Cε (PLCε) is activated downstream of G protein-coupled receptors (GPCRs) and receptor tyrosine kinases (RTKs) through direct interactions with small GTPases. Following stimulation of β-adrenergic receptors (β-ARs), the Rap1A GTPase binds PLCε, translocating the complex to the perinuclear membrane. Although Ras has been reported to allosterically activate the enzyme, it is not known if Rap1A has the same ability or what its molecular mechanism might be. Because the C-terminal Ras association (RA2) domain of PLCε was proposed to the primary binding site for Rap1A, we first confirmed with purified proteins that the RA2 domain is indeed essential for high affinity interactions with Rap1A. However we also showed that the PLCε pleckstrin homology (PH) domain and first two EF hands (EF1/2) are required for Rap1A activation, and identified hydrophobic residues on the surface of the RA2 domain that are necessary for activation but dispensable for GTPase binding. Finally, small angle X-ray scattering (SAXS) showed that Rap1A binding induces and stabilizes discrete conformational states in PLCε variants that are capable of being activated. Considered along with the recent structure of a catalytically active fragment of PLCε, our findings suggest that Rap1A and likely Ras allosterically activate the lipase by promoting and stabilizing interactions between the RA2 domain and the PLC core.

INTRODUCTION

Phospholipase C (PLC) enzymes hydrolyze phosphatidylinositol lipids from cellular membranes in response to diverse cellular signals (1,2). Most hydrolyze phosphatidylinositol-4,5-bisphosphate (PIP_2) at the plasma membrane, producing the second messengers inositol-1,4-5-triphosphate (IP_3) and diacylglycerol (DAG), which increase Ca^{2+} in the cytoplasm and activate PKC, respectively. However, some PLC subfamilies, including PLCε, also hydrolyze other phosphatidylinositol phosphate (PIP) species at internal membrane (3,4). Thus, PLC enzymes can regulate multiple pathways from diverse subcellular locations (1,2).

PLCε is required for maximum Ca^{2+}-induced Ca^{2+} release in the cardiovascular system (5,6). In pathological conditions such as heart failure, PLCε expression and activity are increased, promoting overexpression of genes involved in cardiac hypertrophy (4,7,8). Like other PLCs, PLCε contains a set of conserved core domains, including a pleckstrin homology (PH) domain, four EF hand repeats (EF1-4), a catalytic TIM barrel domain, and a C2 domain (1). However, unique N- and C-terminal regulatory regions flank its PLC core. The N-terminal region contains a CDC25 domain that serves as a guanine nucleotide exchange factor (GEF) for the Rap1A GTPase (9-11), whereas the C-terminal region contains two Ras association (RA) domains known as RA1 and RA2 (Figure 1A). Recent functional analysis of a catalytically active PLCε fragment containing the EF3-RA1 domains confirmed that the N-terminal CDC25 domain, the PH domain and first two EF hands (EF1/2), and that RA2 domain are dispensable for expression and activity. The structure of this fragment revealed that the RA1 domain and the linker connecting the C2 and RA1 domains form extensive interactions with the TIM barrel and C2 domain, suggesting assimilation of the RA1 domain into the catalytic core of the enzyme (12, and Rugema, N.Y, *et al*, *under review*).

The PLCε RA1 and RA2 domains also contribute to subcellular localization and activation via direct interactions with the scaffolding protein mAKAP, and the Rap1A and Ras GTPases (1,4,13-15). Of these, the activation of PLCε by Rap1A has been most studied. Stimulation of β-adrenergic receptors in the cardiovascular system activates adenylyl cyclase, increasing cyclic AMP (cAMP), which in turn activates exchange protein activated by cAMP (Epac). Epac catalyzes nucleotide exchange on Rap1A, which binds the RA2 domain, thereby recruiting and allosterically activating PLCε at the Golgi and perinuclear membranes for phosphatidylinositol-4-phosphate (PI_4P) hydrolysis (4-8). The GEF activity of PLCε for Rap1A then results in the establishment of a feed-forward activation loop (16-18). This

sustained signaling is thought to be one of the key processes underlying pathologic cardiac hypertrophy (3,7,8,19,20).

Although anticipated based on similarities with Ras, Rap1A has not yet been shown to allosterically activate PLCε, and the mechanism by which this would occur is not known. We hypothesized that Rap1A binding works in concert with the membrane surface to promote interdomain contacts in PLCε that stabilize a more catalytically competent state, as has been reported for $G\alpha_q$-dependent activation of the related PLCβ enzyme (21). We found that multiple domains of PLCε, in addition to RA2, are required for binding and activation by constitutively active Rap1A and that hydrophobic residues on the surface of the RA2 domain are essential for Rap1A activation, but not binding. Finally, we used small angle X-ray (SAXS) scattering to show that Rap1A binding induces and stabilizes large scale structural changes in PLCε that turn out to be consistent with the 3D architecture of the enzyme. Together, these results provide new insights into the structure and molecular mechanism of allosteric activation of PLCε by Rap1A.

RESULTS

Rap1A-dependent activation of PLCε requires multiple domains of the lipase. Rap1A-dependent activation of PLCε has been demonstrated in cell-based assays, but not using purified components (17,18,22). As full-length PLCε has not been purified in sufficient quantities for biochemical analysis, we relied on the PLCε PH-COOH variant for these studies (Figure 1A)(23), which retains both RA domains and is thus expected to be responsive to Rap1A. In a liposome-based activity assay, the addition of constitutively active and prenylated $Rap1A^{G12V}$ increased the specific activity of PH-COOH ~3-fold over basal, with a maximum specific activity of 1,900 ± 300 nmol IP_3/min/nmol PLCε variant (Figure 1B, Table 1, Table S1), comparable to the fold activation reported in cells with full-length PLCε (14,22,24). We next quantified the affinity of the $Rap1A^{G12V}$ and PLCε PH-COOH interaction using an AlphaLISA protein interaction assay, and found the EC_{50} to be 0.38 ± 0.3 μM (Figure 1C, Table 1). This is ~30-fold lower than the K_D of 11.5 μM reported for soluble $Rap1A^{G12V}$ and the isolated RA2 domain, as measured by isothermal titration calorimetry (12).

The RA2 domain is expected to be the primary binding site for $Rap1A^{G12V}$, but other regions of PLCε may also be required for activation. Given that the PLC core domains EF3-C2 are essential for basal activity(25-28), we tested whether the PLCε PH domain and EF hands 1/2 (EF1/2) contributed to Rap1A-dependent activation. The PLCe EF3-COOH fragment lacks these elements, and has similar stability and basal activity to PH-COOH (Table 1, Figure S1). As a negative control, we also investigated the PH-C2 variant, which has reduced stability and activity relative to PH-COOH (Table 1, Figure S1)(23) and lacks both RA domains. Indeed, PLCε PH-C2 was not activated by $Rap1A^{G12V}$ at any concentrations tested, consistent with the absence of the RA2 domain (Figure 1B, Table 1). Surprisingly, PLCε EF3-COOH also showed no activation, indicating that the PLCε PH domain and/or EF1/2 are necessary for Rap1A-dependent activation (Figure 1B, Table 1, Table S1).

One explanation for the inability of EF3-COOH to be activated could be impaired binding of $Rap1A^{G12V}$. Using the AlphaLISA protein-interaction assay, we measured the binding affinity of the EF3-COOH and PH-C2 variants for $Rap1A^{G12V}$. The affinity of $Rap1A^{G12V}$ for EF3-COOH was 0.46 ± 0.03 μM, similar to that of PH-COOH (Figure 1C, Table 1). Thus, the inability of $Rap1A^{G12V}$ to activate EF3-COOH is not due to a defect in binding. Interestingly, $Rap1A^{G12V}$ also bound PH-C2 in this assay, despite the absence of the RA2 domain (Figure 1C, Table 1). However, the affinity of the interaction was ~4-fold weaker than that between $Rap1A^{G12V}$ and PH-COOH, with a value of 1.6 ± 1.0 μM (Table 1). Together, these results suggest that while the RA2 domain is required for higher affinity interactions with $Rap1A^{G12V}$, the PLCε core domains also contribute to binding of the GTPase.

Hydrophobic residues on the RA2 domain surface are required for Rap1A-dependent activation. Because our data was consistent with multiple PLCε domains contributing to Rap1A^{G12V} binding and activation, we hypothesized that Rap1A allosterically activates PLCε by promoting or stabilizing potentially long range intra- and interdomain interactions within the lipase. Because both Ras and Rap1A can bind to and activate the enzyme via the RA2 domain, the RA2 domain seems most likely to mediate these interactions. To date, only two residues on the RA2 domain have been characterized with respect to G protein-dependent activation. Mutation of K2150 and/or K2152 (*R. norvegicus* numbering) decrease basal activity and eliminate G protein-dependent activation in cell-based studies (14,22). Based on the structure of activated H-Ras bound to the isolated RA2 domain, K2150 makes an electrostatic interaction with switch II in the GTPase, while K2152 contributes to the local electrostatic environment (12).

We hypothesized that residues involved in allosteric activation on the RA2 domain would likely be surface exposed conserved and hydrophobic residues. Using the H-Ras–RA2 structure as a model for the Rap1A–RA2 interaction (Figure 2A, PDB ID 2C5L (12)), we identified four conserved hydrophobic residues on the surface of the RA2 domain involved in lattice contacts in the crystal structure that did not interact with the GTPase. These residues, Y2155, L2158, L2192, and F2198 (*R. norvegicus* numbering), were individually mutated to alanine in the background of the PLCε PH-COOH variant, and their melting temperature (T_m) and basal activity were determined. As controls, we also expressed, purified, and characterized the PH-COOH K2150 and K2152 point mutants, as they should be insensitive to Rap1A-dependent activation (14,22). The PH-COOH Y2155A, L2158A, L2192A, and F2198A mutants all had T_m values comparable to that of PH-COOH (12,29)(Rugema, N.Y, *et al*, *under review*), and basal specific activities within ~2-fold of PH-COOH (Table 1, Figure S1) suggesting they are properly folded. K2150A and K2152A also had T_m values comparable to that of PH-COOH, but K2150A had ~2-fold lower basal activity, consistent with previous reports (Table 1, Figure S1)(14,22). We then tested the ability of Rap1A^{G12V} to activate the point mutants in a liposome-based activity assay. The K2150 and K2152A mutants were insensitive to activation by Rap1A^{G12V}, consistent with their proposed role in binding GTPases (Figure 2B, Table 1)(14,22). Mutation of the hydrophobic surface residues also eliminated Rap1A^{G12V}-dependent activation (Figure 2C, Table 1, Table S1). Thus, the hydrophobic residues appear to play a critical role in this mechanism.

PLCε RA2 mutants are not impaired in Rap1A^{G12V} binding. Mutations to conserved residues on the RA2 surface eliminated Rap1A^{G12V}-dependent activation. The K2150 and K2152 mutants would be expected to be impaired in Rap1A binding, leading to loss of activation. However, the loss of activation for the hydrophobic point mutants could be due to defects in Rap1A binding or loss of long-range allosteric contacts of RA2 with other domains. We therefore returned to the AlphaLISA protein-interaction assay to measure the binding affinity of the PLCe PH-COOH RA2 mutants for Rap1A^{G12V}. The hydrophobic RA2 point mutants L2158A (EC_{50}: 0.44 ± 0.15 μM), L2192A (EC_{50}: 0.40 ± 0.42 μM), and F2198A (EC_{50}: 0.39 ± 0.25 μM) all bound Rap1A^{G12V} with comparable affinity to that of PH-COOH (Table 1, Figure 3A). PH-COOH Y2155A had a slightly higher affinity for Rap1A^{G12V}, with an EC_{50} of 0.29 ± 0.14 μM (Figure 3A, Table 1). The loss of Rap1A-dependent activation observed for the hydrophobic point mutants is therefore not due to impaired GTPase binding. Similar trends were observed for the K2150A and K2152A mutants, where PH-COOH K2150A bound Rap1A^{G12V} with an EC_{50} of 0.49 ± 0.14 μM (Figure 3B, Table 1). This finding is consistent with a prior study, wherein mutation of this lysine to leucine in the RA2 domain did not perturb the binding affinity for H-Ras (12). PH-COOH K2152A had an EC_{50} for Rap1A similar to that of PH-COOH (EC_{50}: 0.45 ± 0.11 μM, Figure 3B, Table 1). Thus, the lysine residues appear to be dispensable for binding, at least in the context of PLCε PH-COOH and our assay conditions.

Rap1A^{G12V} binding to PLCε induces and stabilizes unique conformational states. Our domain deletion and site-directed mutagenesis analyses identified roles for the PH domain, EF1/2, and the hydrophobic residues on the RA2 surface in Rap1A^{G12V}-dependent activation. To gain structural insight into how these

elements contribute to Rap1A^{G12V} binding and/or activation. However, we have yet to obtain a crystal structure for this fragment. We therefore used SAXS to compare the solution structures of the PLCε PH-COOH and EF3-COOH variants alone and in complex with Rap1A^{G12V}. These variants were chosen because they form stable complexes with Rap1A^{G12V} that can be isolated by size exclusion chromatography, but only PH-COOH has increased lipase activity upon binding of the GTPase (Figure 1, Table 1).

We first compared the SAXS solution structure of the Rap1A^{G12V}–PH-COOH complex with that previously determined for PLCε PH-COOH, which had a globular structure with extended features likely due to the flexibly connected PH, EF1/2, and RA2 domains (Figures 4, 5A, Table 2, Table S2, Figure S2)(23,30). The Rap1A^{G12V}–PH-COOH sample was more complex, and contained three minor components that partially overlapped the major complex peak in the SEC-SAXS elution profile (Figure S2). To identify the region corresponding to Rap1A^{G12V}–PH-COOH, evolving factor analysis (EFA) was used to deconvolute the data (Figure S3)(32,33). The Rap1A^{G12V}–PH-COOH complex had an R_g of 42.4 ± 0.12 Å (Figure 4D, E) and a D_{max} of ~165 Å, with a largely globular structure with some extended features (Figure 4). Further analysis of the samples, shown in the dimensionless Kratky plot, reveals conformational changes due to Rap1A^{G12V} binding (Figure 5B). In this plot, compact, globular proteins have a bell-shaped curve that converges to the qR_g axis at high values, whereas elongated and more rigid structures exhibit curves that extend out to higher qR_g, and highly flexible structures do not converge at all (31). The data for the Rap1A^{G12V}–PH-COOH complex shows the overall structure is more compact and/or less flexible than PH-COOH alone, as evidenced by the curve being more bell-shaped and converging to zero at lower values of qRg (Figure 5B).

We next compared the solution structures of PLCε EF3-COOH alone and in complex with Rap1A^{G12V}. EF3-COOH was also monomeric and monodisperse in solution, with an R_g of 41.9 ± 0.43 Å and a D_{max} of ~175 Å (Figure 4G-I, Table 2, Table S2, Figure S2). Its P(r) function is also consistent with the protein having a mostly globular structure with a modest degree of extendedness and/or flexibility (Figures 4I, 5C). In contrast, the solution structure of the Rap1A^{G12V}–EF3-COOH complex differs substantially from EF3-COOH. The complex had an R_g of 36.8 ± 0.5 Å (Figure 4J, K, Table S2, Figure S2), and its P(r) function reveals a much more compact and globular structure, as shown in the more bell-shaped function and a ~30 Å decrease in D_{max} to ~145 Å (Figures 4, 5, Table 2). This is further highlighted in the dimensionless Kratky plot, which clearly show that Rap1A^{G12V} binding induces conformational changes that result in a more compact, stable structure (Figure 5D). Because EF3-COOH is not activated by Rap1A^{G12V} (Figure 1, Table 1), this more condensed state may represent a nonproductive conformation of the complex.

DISCUSSION

The PLCε RA domains are very similar in structure, but have evolved different functional roles in the enzyme (1,4,12-15, Rugema, N.Y, *et al*, *under review*). The RA1 domain, together with the loop connecting the C2 and RA1 domains, forms extensive contacts with EF hands 3/4 (EF3/4), the TIM barrel, and the C2 domain that are important for stability and activity (Rugema, N.Y, *et al*, *under review*). RA1 also interacts with muscle-specific A-kinase anchoring protein (mAKAP), a scaffolding protein at the Golgi, helping to localize PLCε to internal membranes (15). In contrast, the contribution of the RA2 domain to basal activity is unclear, as its deletion has been reported to either activate or inhibit basal activity (12,14). The RA2 domain is the primary binding site for activated Rap1A and Ras GTPases, as its deletion or mutation of two highly conserved lysines (*R. norvegicus* PLCε K2150 and K2152, Figure 2A) eliminates G protein-dependent activation in cells (12,14,16). Interestingly, mutation of K2150 alone is sufficient to decrease basal activity ~50% in cells (14,16). NMR and biochemical studies have demonstrated RA2 is flexibly connected to RA1, and does not stably associate with the PLCε core domains (12, Rugema, N.Y, *et al*, *under review*). However, how GTPase binding to this domain is translated into increased lipase activity is poorly understood. Given that all known activators PLCε are

lipidated, membrane localization is one aspect of the activation mechanism. However, membrane association alone is insufficient to fully stimulate lipase activity. For example, a PLCε variant bearing a -CAAX motif at its C-terminus to drive plasma membrane localization had increased lipase activity, but was further stimulated ~4-fold in the presence of activated Ras, suggesting that the activation mechanism mediated by small GTPases must also have an allosteric component (12).

In this work, we used a series of purified PLCε domain deletion variants and point mutants to investigate the allosteric component of the activation mechanism. We have shown constitutively activate Rap1A binds to and increases the lipase activity of the PLCε PH-COOH *in vitro* to a similar extent as full-length PLCε in cells (Figure 1)(17,18,22). We also found the PH domain and EF1/2 are required for Rap1A-dependent activation, but not binding, as EF3-COOH bound $Rap1A^{G12V}$ with affinity similar to PH-COOH but failed to show any increase in lipase activity (Figure 1, Table 1). Surprisingly, PH-C2, which lacks both RA domains, bound the GTPase, albeit with a ~4-fold decrease in affinity (Figures 1, 2, Table 1). Together, these findings support a model in which the binding of Rap1A is a collaborative event involving multiple domains of PLCε.

We then attempted to identify conserved residues in the RA2 domain, which is of known structure, that could be involved in intramolecular interactions with the PLCe core domains upon Rap1A binding. Guided by the previously determined crystal structure of the H-Ras–RA2 complex (Figure 2A, PDB ID 2C5L(12)), we identified four conserved, solvent-exposed, hydrophobic resides on RA2 that are distant from the predicted Rap1A binding site. Mutation of Y2155, L2158, L2192, or F2198 to alanine eliminated $Rap1A^{G12V}$-dependent activation without changing the affinity for $Rap1A^{G12V}$ (Figure 2, 3, Table 1). One explanation for these results is that the conserved, hydrophobic residues on the RA2 surface interact with or stabilize intramolecular contacts between the RA2 domain and the PLCε core. As these residues are not involved in Rap1A binding, these intramolecular interactions may function to communicate the fact that GTPase is bound to the rest of the lipase.

Our study identifies roles for the PLCε PH domain, EF1/2, and conserved hydrophobic residues on the RA2 surface as being critical for Rap1A-dependent activation. These domains are distant in the primary structure of PLCε (Figure 1A), but are situated in relatively close spatial proximity based on the recent structure of the PLCε EF3-RA1 fragment (Rugema, N.Y, *et al*, *under review*). To gain structural insights into how these structural elements could contribute to activation, we used SAXS to compared the solution structures of PLCε PH-COOH and EF3-COOH alone and in complex with $Rap1A^{G12V}$. This comparison allows identification of large-scale conformational changes, changes in shape (globular vs. extended), as well as differences in flexibility (Figures 4, 5, Table 2, Table S2). The PLCε variants alone had similar globular structures with some extended/flexible features. The binding of $Rap1A^{G12V}$ to either variant induced conformational changes that resulted in more ordered, less flexible structures (Figures 4, 5). However, these two Rap1A-bound complexes differ substantially from one another, as $Rap1A^{G12V}$ binding to EF3-COOH decreased the maximum diameter of the complex by ~20 Å and stabilized a more compact, globular structure (Figures 4, 5, Table 2). Because the lipase activity of EF3-COOH is not increased by Rap1A, this solution structure cannot represent in the active state. In contrast, $Rap1A^{G12V}$ binding to PH-COOH did not appreciably change the maximum diameter of the complex, but did lead to a structure that is more globular and less flexible than PH-COOH alone (Figures 4, 5). These results indicate that Rap1A binding may stabilize the interactions between the Rap1A-bound RA2 domain and the PLCε core.

Overall, our results provide the first direct structural evidence about the nature of the allosteric component of Rap1A-dependent (and likely Ras-dependent) activation of PLCε, and reveal that activation involves substantial conformational changes within the lipase. Whereas the PLCε RA2 domain is required for highest affinity binding to the Rap1A, activation is also dependent on the PH domain, EF1/2, and hydrophobic surface residues on the RA2 domain. These observations are consistent with the following model (Figure 6). Because the RA2 domain is flexibly tethered to RA1, it may transiently interact with rest the of PLCε core in solution. These interactions are insufficient to alter the thermal stability or increase basal activity. Upon Rap1A binding to the RA2 domain, this complex could stabilize interactions

with other domains in PLCε, most likely via the hydrophobic residues present on the surface of RA2 with the PH domain and/or EF1/2, based on the crystal structure of PLCε (Rugema, N.Y, *et al*, *under review*). Finally, the membrane itself contributes to Rap1A-dependent activation in several possible ways. Although the regions responsible for membrane association in PLCε have not yet been identified, the enzyme has measurable basal activity, and thus can at least transiently interact with the membrane (14). Finally, Rap1A is prenylated and thus, along with any other membrane binding element, likely helps to orient the lipase active site at the membrane for maximum lipid hydrolysis. Future studies that provide higher resolution insights into the interactions between the RA2 domain and the PLCε core, alone and in complex with activated Rap1A, will be essential step in elucidating a complete picture of this process and new opportunities for therapeutic development that target activation of PLCε by small GTPases.

EXPERIMENTAL PROCEDURES

Protein expression, purification, and mutagenesis of PLCε variants. cDNAs encoding N-terminally His-tagged *R. norvegicus* PLCε variants were subcloned into pFastBac HTA (PH-COOH: residues 837-2281, PH-C2: 832-1972, and EF3-COOH: 1284-2281). Site-directed mutagenesis in the PH-COOH background was performed using the QuikChange Site-Directed Mutagenesis Kit (Stratagene) or the Q5 Site-Directed Mutagenesis Kit (NEB). All subcloned PLCε variants contained an N-terminal His-tag and TEV cleavage site, and were sequenced over the entire coding region. The proteins were expressed and purified as previously described (23), with some modifications for the PLCε EF3-COOH used in the SAXS experiments. Briefly, after elution from an Ni-NTA column, PLCε EF3-COOH was incubated with 5% w/w TEV protease to remove the N-terminal His-tag and dialyzed overnight against 1.5 L of buffer containing 20 mM HEPES pH 8.0, 50 mM NaCl, 2 mM DTT, 0.1 mM EDTA, and 0.1 mM EGTA at 4 °C. The dialysate was applied to Roche cOmplete NiNTA resin or a GE HisTrap, and the flow-through containing the TEV-cleaved EF3-COOH was collected and passed over the column two more times. The protein in the collected flow-through was then purified as previously described (23).

Expression and purification of prenylated Rap1A^{G12V}·GTP. cDNA encoding N-terminally His-tagged constitutively active *H. sapiens* Rap1A (Rap1A^{G12V}) was subcloned into pFastBac HTA. N-terminally GST-tagged *H. sapiens* Rap1A^{G12V} was generated using the Q5 Site-Directed Mutagenesis Kit and subcloned into pFastbac Dual. Proteins were expressed in baculovirus-infected High5 cells. Cell pellets were resuspended in lysis buffer containing 20 mM HEPES pH 8.0, 100 mM NaCl, 10 mM β-mercaptoethanol, 0.1 mM EDTA, 10 mM NaF, 20 mM $AlCl_3$, 0.1 mM LL, 0.1 mM PMSF, and 20 μM GTP and lysed via dounce on ice. The lysate was centrifuged for 1 h at 100,000 x *g*, and the pellet was resuspended in lysis buffer supplemented with 1% sodium cholate, dounced on ice, and solubilized at 4 °C for 1 h. The sample was then centrifuged for 1 h at 100,000 x *g*, and the supernatant was diluted two-fold with lysis buffer.

His-tagged Rap1A^{G12V} was loaded on a Ni-NTA column pre-equilibrated with lysis buffer, and first washed with lysis buffer containing 10 mM imidazole and 0.2% cholate, followed by a second wash with lysis buffer supplemented with 10 mM imidazole and 10 mM CHAPS (3-[(3-cholamidopropyl)dimethylammonio]-1-propanesulfonate). The protein was eluted with lysis buffer containing 250 mM imidazole pH 8.0 and 10 mM CHAPS. GST-Rap1A^{G12V} was loaded onto a glutathione column pre-equilibrated with lysis buffer. The column was washed with lysis buffer containing 0.2% cholate, followed by lysis buffer supplemented with 10 mM CHAPS. GST-Rap1A^{G12V} was eluted with lysis buffer supplemented with 20 mM reduced glutathione and 10 mM CHAPS. His-tagged Rap1A^{G12V} or GST-Rap1A^{G12V} were then concentrated and applied to tandem Superdex S200 columns pre-equilibrated with G protein S200 buffer (20 mM HEPES pH 8.0, 50 mM NaCl, 1 mM $MgCl_2$, 2 mM DTT, 10 mM CHAPS, and 20 μM GTP). Fractions containing purified protein were identified by SDS-PAGE, pooled, concentrated, and flash frozen in liquid nitrogen. Rap1A^{G12V} used for activation assays was purified in modified G protein S200 buffer containing 1 mM CHAPS.

For SAXS experiments and AlphaLISA competitive binding assays, His-tagged Rap1A^{G12V} was incubated with 5% w/w TEV protease and dialyzed overnight in 1.5 L of dialysis buffer containing 20 mM HEPES pH 8.0, 50 mM NaCl, 1 mM $MgCl_2$, 10 mM β-mercaptoethanol, 1 mM CHAPS, and 20 μM GTP at 4 °C. The dialysate was applied to a Ni-NTA column, and the flow-through containing cleaved Rap1A^{G12V} was collected and passed over the column two more times. The flow-through was collected, concentrated to 1 mL, applied to tandem Superdex S200 columns and purified as described above.

Differential scanning fluorimetry (DSF). Melting temperatures (T_m) of PLCε variants were determined as previously described (23,29). A final concentration of 0.5 mg/mL was used for each PLCε variant. At least three independent experiments were performed in duplicate.

PLCε activity assays. All activity assays were carried out using [^{3}H]-PIP_2 as the substrate. Basal activity of PLCε variants was measured as previously described (23). Briefly, 200 μM phosphatidylethanolamine, 50 μM PIP_2, and ~4,000 cpm [^{3}H]-PIP_2 were mixed, dried under nitrogen, and resuspended by sonication in buffer containing 50 mM HEPES pH 7, 80 mM KCl, 2 mM EGTA, and 1 mM DTT. Enzyme activity was measured at 30 °C in 50 mM HEPES pH 7, 80 mM KCl, 15 mM NaCl, 0.83 mM MgCl2, 3 mM DTT, 1 mg/mL bovine serum albumin (BSA), 2.5 mM EGTA, 0.2 mM EDTA, and ~500 nM free Ca^{2+}. PLCε PH-COOH and EF3-COOH were assayed at a final concentration of 0.075 ng/μL and PH-C2 at 0.1-1ng/μL (23). The PH-COOH K2150A, K2152A, Y2155A, L2158A, L2192A, and F2198A mutants were assayed at a final concentration of 0.5 ng/μL. Control reactions contained everything except free Ca^{2+}. Reactions were quenched by addition of 200 μL 10 mg/mL BSA and 10% (w/v) ice-cold trichloroacetic acid and centrifuged. Free [^{3}H]-IP_3 in the supernatant was quantified by scintillation counting. All assays were performed at least three times in duplicate.

Rap1A^{G12V}-dependent increases in PLCε lipase activity were measured using the same approach with some modifications. The liposomes were first incubated with increasing concentrations of Rap1A^{G12V}·GTP in 50 mM HEPES pH 7.0, 3 mM EGTA, 1 mM EDTA, 100 mM NaCl, 5 mM $MgCl_2$, 3 mM DTT, and 390 μM CHAPS at 30 °C for 30 min. The reaction was initiated by addition of the PLCε variant, incubated at 30 °C for 8 min, and processed as described above. All activation assays were performed in duplicate with protein from at least two independent purifications.

AlphaLISA Competitive Binding Assay. GST-Rap1A^{G12V} and His-tagged PLCε variants were immobilized on AlphaScreen glutathione donor beads and nickel chelate AlphaLISA acceptor beads, respectively (PerkinElmer). Binding between bead-bound Rap1A^{G12V} and PLCε variants results in luminescence. Addition of increasing concentrations of untagged Rap1A^{G12V} competes for binding to the PLCε variant, thereby decreasing the signal. Negative controls included the donor and acceptor beads in the absence of proteins, donor beads with GST-Rap1A^{G12V} and acceptor beads, and acceptor beads with PLCε variants and donor beads. All reactions were carried out in white 384-well ProxiPlates (PerkinElmer) in buffer containing 20 mM HEPES pH 8, 50 mM NaCl, 2 mM DTT, 0.1 mM EDTA, 0.1 mM EGTA, 1 mM $MgCl_2$, 0.5 mM $CaCl_2$, 40 μM GTP, and ~0.02% CHAPS. 500 nM GST-Rap1A^{G12V} was preincubated with serial dilutions of untagged Rap1A^{G12V} (0 – 10 μM) and 50 nM PLCε variant, and incubated on ice for 1 h. 20 μg/mL of Ni-NTA AlphaLISA acceptor beads were added to each well and incubated for 1 h in the dark at room temperature, followed by 20 μg/mL of the AlphaScreen glutathione donor beads to each well, and incubated for another 1 h in the dark at room temperature. Assay plates were read using an EnVision plate reader (PerkinElmer) or a Spark10 multimode microplate reader (Tecan) and analyzed using GraphPad Prism v.8.0.1, with automatic outlier rejection. All assays were performed at least three times in duplicate.

Formation and isolation of the Rap1A^{G12V}–PLCε variant complexes. A 1:3 or 1:5 molar ratio of PLCε PH-COOH or EF3-COOH to Rap1A^{G12V}, supplemented with 0.5 mM $CaCl_2$, was incubated on ice for 30

min before being applied to a Superdex S200 column pre-equilibrated with complex S200 buffer (20 mM HEPES pH 8, 50 mM NaCl, 2 mM DTT, 0.1 mM EDTA, 0.1 mM EGTA, 1 mM $MgCl_2$, 0.5 mM $CaCl_2$ and 40 μM GTP). Fractions containing the purified complex were identified by SDS-PAGE, pooled, and concentrated for use in SAXS experiments.

SAXS Data Collection and Analysis. PLCε PH-COOH was previously characterized by SAXS (23). PLCε EF3-COOH, the $Rap1A^{G12V}$–PLCε PH-COOH complex, and the $Rap1A^{G12V}$–PLCε EF3-COOH complex were diluted to final concentrations of 2-3 mg/mL in S200 buffer (EF3-COOH) or complex S200 buffer, and centrifuged at 16,000 x *g* for 5 min at 4 ºC prior to data collection. Size exclusion chromatography (SEC)-SAXS was performed at the BioCAT beamline at Sector 18 of the Advanced Photon Source (Table S1).

Protein samples were eluted from a Superdex 200 Increase 10/300 GL column using an ÄKTA Pure FPLC (GE Healthcare) at a flow rate of 0.7 mL/min. The eluate passed through a UV monitor followed by a SAXS flow cell consisting of a quartz capillary. The data were collected in two different setups at the beamline. The PH-COOH, EF3-COOH, and EF3-COOH complex data were collected in a 1.5 mm ID quartz capillary with 10 μm walls. The PH-COOH complex data was collected in a 1.0 mm ID quartz capillary with 50 μm using the coflow sample geometry (35) to prevent radiation damage. Scattering intensity was recorded using Pilatus3 X 1M detector (Dectris) placed ~3.7 m from the sample using 12 KeV X-rays (1.033 Å wavelength) and a beam size of 160 x 75 μm, giving an accessible q range of ~0.004 $Å^{-1}$ to 0.36 $Å^{-1}$. Data was collected every 2 s with 0.5 s exposure times. Data in regions flanking the elution peak were averaged to create buffer blanks which were subsequently subtracted from exposures selected from the elution peak to create the final scattering profiles (Figure S2). BioXTAS RAW 1.4.0(33) was used for data processing and analysis. For the $Rap1A^{G12V}$–PLCe PH-COOH complex, the four components present in the sample were deconvoluted using evolving factor analysis (EFA, Figure S3)(32)) as implemented in BIOXTAS RAW(33). The radius of gyration (R_g) of individual frames were plotted with the scattering chromatograms, which plot integrated intensity of individual exposures as a function of frame number, and used to help determine appropriate sample ranges for subtraction. PRIMUS (36)was used to calculate the R_g, $I_{(0)}$, and D_{max} for both samples. GNOM (37) was used within PRIMUS to generate the pair distance distribution (P(r)) functions via an indirect Fourier transform (IFT) method.

Graphical plots were generated from buffer-subtracted averaged data (scattering profile and Guinier plots)(38) or IFT data (P(r) plots) and plotted using GraphPad Prism v.8.0.1. SAXS data are presented in accordance with the publication guidelines for small angle scattering data(39).

Statistical Methods. GraphPad Prism v.8.0.1 was used to generate all plots. One-way ANOVA was performed with Prism v.8.0.1 followed by Dunnett's post-hoc multiple comparisons vs. PLCε PH-COOH, as noted in figure captions. All error bars represent standard deviation.

SUPPORTING INFORMATION

Supporting Table 1. Minimum and Maximum Specific Activities under $Rap1A^{G12V}$ activating conditions

Supporting Table 2. SAXS Molecular Weight Estimations for PLCε PH-COOH and EF3-COOH alone and in complex with $Rap1A^{G12V}$.

Supporting Figure 1. Characterization of the PLCε domain deletion variants and RA2 point mutants

Supporting Table 3. SAXS Data Collection and Analysis Parameters

Supporting Figure 2. Size exclusion chromatography (SEC-SAXS) scattering chromatograms for PLCε variants alone and in complex with $Rap1A^{G12V}$.

Supporting Figure 3 Deconvolution of the $Rap1A^{G12V}$–PH-COOH elution peak using evolving factor analysis (EFA).

AUTHOR CONTRIBUTIONS

M.S. and A.M.L. designed the experimental approach. M.S., E.E.G.-K, A.F.S., and A.T.M. cloned, expressed, and purified all PLCε and Rap1A proteins. M.S., E.E.G.-K., and I.J.F. performed DSF and activity assays. M.S. and A.F.S. performed direct binding assays, and isolated Rap1A–PLCε complexes for SAXS analysis. J.B.H. assisted with SAXS experiments, data analysis, and processing. M.S., E.E.G.-K., J.B.H., and A.M.L. wrote the manuscript.

FUNDING SOURCES

This work is supported by an American Heart Association Predoctoral Fellowship Grant 18PRE33990057 (M.S.), American Heart Association Scientist Development Grant 16SDG29920017 (A.M.L.), an American Cancer Society Institutional Research Grant (IRG-14-190-56) to the Purdue University Center for Cancer Research (A.M.L.), and NIH 1R01HL141076-01 (A.M.L.).

ACKNOWLEDGMENTS

We thank S. Chakravarthy (APS BioCAT) for assistance with SAXS data collection and analysis. Use of the Advanced Photon Source, an Office of Science User Facility operated for the U. S. Department of Energy (DOE) Office of Science by Argonne National Laboratory, was supported by the U.S. DOE under Contract Number DE-AC02-06CH11357. This project was supported by grant 9 P41 GM103622 from the National Institute of General Medical Sciences of the National Institutes of Health. Use of the Pilatus 3 1M detector was provided by grant 1S10OD018090-01 from NIGMS.

The content is solely the responsibility of the authors and does not necessarily represent the official views of the National Institute of General Medical Sciences or the National Institutes of Health.

ABBREVIATIONS

PLC, Phospholipase C; RA, Ras association; DAG, diacylglycerol; IP_3, inositol-1,4,5-triphopshate; PKC, protein kinase C; CHAPS, 3-[(3-cholamidopropyl)dimethyl-ammonio]-1-propane sulfonate; GEF, guanine exchange factor; GPCR, G protein-coupled receptor; RTK, receptor tyrosine kinase; cAMP, cyclic AMP; Epac, exchange protein activated by cAMP; PIP, phosphatidylinositol phosphate; PIP_2, phosphatidylinositol (4,5)-bisphosphate; PE, phosphatidylethanolamine; PH, pleckstrin homology; TIM, triose-phosphate isomerase; RA, Ras association; PI_4P, phosphatidylinositol-4-phosphate; DSF, differential scanning fluorimetry; SAXS, small angle X-ray scattering; size exclusion chromatography, SEC

REFERENCES

1. Kadamur, G., and Ross, E. M. (2013) Mammalian phospholipase C. *Annu Rev Physiol* **75**, 127-154
2. Gresset, A., Sondek, J., and Harden, T. K. (2012) The phospholipase C isozymes and their regulation. *Subcell Biochem* **58**, 61-94
3. de Rubio, R. G., Ransom, R. F., Malik, S., Yule, D. I., Anantharam, A., and Smrcka, A. V. (2018) Phosphatidylinositol 4-phosphate is a major source of GPCR-stimulated phosphoinositide production. *Science Signaling* **11**
4. Smrcka, A. V., Brown, J. H., and Holz, G. G. (2012) Role of phospholipase Cε in physiological phosphoinositide signaling networks. *Cell Signal* **24**, 1333-1343
5. Oestreich, E. A., Malik, S., Goonasekera, S. A., Blaxall, B. C., Kelley, G. G., Dirksen, R. T., and Smrcka, A. V. (2009) Epac and phospholipase Cε regulate Ca^{2+} release in the heart by activation of protein kinase Cε and calcium-calmodulin kinase II. *J Biol Chem* **284**, 1514-1522
6. Oestreich, E. A., Wang, H., Malik, S., Kaproth-Joslin, K. A., Blaxall, B. C., Kelley, G. G., Dirksen, R. T., and Smrcka, A. V. (2007) Epac-mediated activation of phospholipase Cε plays a critical role in beta-adrenergic receptor-dependent enhancement of Ca^{2+} mobilization in cardiac myocytes. *J Biol Chem* **282**, 5488-5495
7. Zhang, L., Malik, S., Pang, J., Wang, H., Park, K. M., Yule, D. I., Blaxall, B. C., and Smrcka, A. V. (2013) Phospholipase cepsilon hydrolyzes perinuclear phosphatidylinositol 4-phosphate to regulate cardiac hypertrophy. *Cell* **153**, 216-227
8. Wang, H., Oestreich, E. A., Maekawa, N., Bullard, T. A., Vikstrom, K. L., Dirksen, R. T., Kelley, G. G., Blaxall, B. C., and Smrcka, A. V. (2005) Phospholipase C ε modulates β-adrenergic receptor-dependent cardiac contraction and inhibits cardiac hypertrophy. *Circ Res* **97**, 1305-1313
9. Jin, T. G., Satoh, T., Liao, Y., Song, C., Gao, X., Kariya, K., Hu, C. D., and Kataoka, T. (2001) Role of the CDC25 homology domain of phospholipase Cε in amplification of Rap1-dependent signaling. *J Biol Chem* **276**, 30301-30307
10. Satoh, T., Edamatsu, H., and Kataoka, T. (2006) Phospholipase Cε guanine nucleotide exchange factor activity and activation of Rap1. *Methods Enzymol* **407**, 281-290
11. Dusaban, S. S., Kunkel, M. T., Smrcka, A. V., and Brown, J. H. (2015) Thrombin Promotes Sustained Signaling and Inflammatory Gene Expression through the CDC25 and Ras Associating Domains of Phospholipase C-epsilon. *J Biol Chem* **290**, 26776-26783
12. Bunney, T. D., Harris, R., Gandarillas, N. L., Josephs, M. B., Roe, S. M., Sorli, S. C., Paterson, H. F., Rodrigues-Lima, F., Esposito, D., Ponting, C. P., Gierschik, P., Pearl, L. H., Driscoll, P. C., and Katan, M. (2006) Structural and mechanistic insights into ras association domains of phospholipase C ε. *Mol Cell* **21**, 495-507
13. Wing, M. R., Bourdon, D. M., and Harden, T. K. (2003) PLC-ε: a shared effector protein in Ras-, Rho-, and Gαβγ-mediated signaling. *Mol Interv* **3**, 273-280
14. Kelley, G. G., Reks, S. E., Ondrako, J. M., and Smrcka, A. V. (2001) Phospholipase Cε: a novel Ras effector. *EMBO J* **20**, 743-754
15. Zhang, L., Malik, S., Kelley, G. G., Kapiloff, M. S., and Smrcka, A. V. (2011) Phospholipase C ε scaffolds to muscle-specific A kinase anchoring protein (mAKAPβ) and integrates multiple hypertrophic stimuli in cardiac myocytes. *J Biol Chem* **286**, 23012-23021
16. Kelley, G. G., Kaproth-Joslin, K. A., Reks, S. E., Smrcka, A. V., and Wojcikiewicz, R. J. (2006) G-protein-coupled receptor agonists activate endogenous phospholipase Cε and phospholipase Cβ3 in a temporally distinct manner. *J Biol Chem* **281**, 2639-2648
17. Edamatsu, H., Satoh, T., and Kataoka, T. (2006) Ras and Rap1 activation of PLCepsilon lipase activity. *Methods Enzymol* **407**, 99-107
18. Song, C., Satoh, T., Edamatsu, H., Wu, D., Tadano, M., Gao, X., and Kataoka, T. (2002) Differential roles of Ras and Rap1 in growth factor-dependent activation of phospholipase C epsilon. *Oncogene* **21**, 8105-8113

19. Nash, C. A., Brown, L. M., Malik, S., Cheng, X., and Smrcka, A. V. (2018) Compartmentalized cyclic nucleotides have opposing effects on regulation of hypertrophic phospholipase Cepsilon signaling in cardiac myocytes. *J Mol Cell Cardiol*
20. Nash, C. A., Wei, W., Irannejad, R., and Smrcka, A. V. (2019) Golgi localized beta1-adrenergic receptors stimulate Golgi PI4P hydrolysis by PLCepsilon to regulate cardiac hypertrophy. *eLife* **8**
21. Lyon, A. M., Dutta, S., Boguth, C. A., Skiniotis, G., and Tesmer, J. J. (2013) Full-length Galpha(q)-phospholipase C-beta3 structure reveals interfaces of the C-terminal coiled-coil domain. *Nat Struct Mol Biol* **20**, 355-362
22. Kelley, G. G., Reks, S. E., and Smrcka, A. V. (2004) Hormonal regulation of phospholipase Cε through distinct and overlapping pathways involving G_{12} and Ras family G-proteins. *Biochem J* **378**, 129-139
23. Garland-Kuntz, E. E., Vago, F. S., Sieng, M., Van Camp, M., Chakravarthy, S., Blaine, A., Corpstein, C., Jiang, W., and Lyon, A. M. (2018) Direct observation of conformational dynamics of the PH domain in phospholipases C and beta may contribute to subfamily-specific roles in regulation. *J Biol Chem* **293**, 17477-17490
24. Khrenova, M. G., Mironov, V. A., Grigorenko, B. L., and Nemukhin, A. V. (2014) Modeling the role of G12V and G13V Ras mutations in the Ras-GAP-catalyzed hydrolysis reaction of guanosine triphosphate. *Biochemistry* **53**, 7093-7099
25. Essen, L. O., Perisic, O., Cheung, R., Katan, M., and Williams, R. L. (1996) Crystal structure of a mammalian phosphoinositide-specific phospholipase C δ. *Nature* **380**, 595-602
26. Zhang, W., and Neer, E. J. (2001) Reassembly of phospholipase C-β2 from separated domains: analysis of basal and G protein-stimulated activities. *J Biol Chem* **276**, 2503-2508
27. Seifert, J. P., Wing, M. R., Snyder, J. T., Gershburg, S., Sondek, J., and Harden, T. K. (2004) RhoA activates purified phospholipase C-ε by a guanine nucleotide-dependent mechanism. *J Biol Chem* **279**, 47992-47997
28. Seifert, J. P., Zhou, Y., Hicks, S. N., Sondek, J., and Harden, T. K. (2008) Dual activation of phospholipase C-ε by Rho and Ras GTPases. *J Biol Chem* **283**, 29690-29698
29. Mezzasalma, T. M., Kranz, J. K., Chan, W., Struble, G. T., Schalk-Hihi, C., Deckman, I. C., Springer, B. A., and Todd, M. J. (2007) Enhancing recombinant protein quality and yield by protein stability profiling. *J Biomol Screen* **12**, 418-428
30. Korasick, D. A., and Tanner, J. J. (2018) Determination of protein oligomeric structure from small-angle X-ray scattering. *Protein science : a publication of the Protein Society* **27**, 814-824
31. Durand, D., Vives, C., Cannella, D., Perez, J., Pebay-Peyroula, E., Vachette, P., and Fieschi, F. (2010) NADPH oxidase activator p67(phox) behaves in solution as a multidomain protein with semi-flexible linkers. *J Struct Biol* **169**, 45-53
32. Meisburger, S. P., Taylor, A. B., Khan, C. A., Zhang, S., Fitzpatrick, P. F., and Ando, N. (2016) Domain Movements upon Activation of Phenylalanine Hydroxylase Characterized by Crystallography and Chromatography-Coupled Small-Angle X-ray Scattering. *Journal of the American Chemical Society* **138**, 6506-6516
33. Hopkins, J. B., Gillilan, R. E., and Skou, S. (2017) BioXTAS RAW: improvements to a free open-source program for small-angle X-ray scattering data reduction and analysis. *Journal of applied crystallography* **50**, 1545-1553
34. Hicks, S. N., Jezyk, M. R., Gershburg, S., Seifert, J. P., Harden, T. K., and Sondek, J. (2008) General and versatile autoinhibition of PLC isozymes. *Mol Cell* **31**, 383-394
35. Kirby, N., Cowieson, N., Hawley, A. M., Mudie, S. T., McGillivray, D. J., Kusel, M., Samardzic-Boban, V., and Ryan, T. M. (2016) Improved radiation dose efficiency in solution SAXS using a sheath flow sample environment. *Acta crystallographica. Section D, Structural biology* **72**, 1254-1266
36. Konarev, P. V., Volkov, V. V., Sokolova, A. V., Koch, M. H. J., and Svergun, D. I. (2003) PRIMUS: a Windows PC-based system for small-angle scattering data analysis. *Journal of applied crystallography* **36**, 1277-1282

37. Svergun, D. I. (1992) Determination of the Regularization Parameter in Indirect-Transform Methods Using Perceptual Criteria. *Journal of applied crystallography* **25**, 495-503
38. Franke, D., Petoukhov, M. V., Konarev, P. V., Panjkovich, A., Tuukkanen, A., Mertens, H. D. T., Kikhney, A. G., Hajizadeh, N. R., Franklin, J. M., Jeffries, C. M., and Svergun, D. I. (2017) ATSAS 2.8: a comprehensive data analysis suite for small-angle scattering from macromolecular solutions. *Journal of applied crystallography* **50**, 1212-1225
39. Trewhella, J., Duff, A. P., Durand, D., Gabel, F., Guss, J. M., Hendrickson, W. A., Hura, G. L., Jacques, D. A., Kirby, N. M., Kwan, A. H., Perez, J., Pollack, L., Ryan, T. M., Sali, A., Schneidman-Duhovny, D., Schwede, T., Svergun, D. I., Sugiyama, M., Tainer, J. A., Vachette, P., Westbrook, J., and Whitten, A. E. (2017) 2017 publication guidelines for structural modelling of small-angle scattering data from biomolecules in solution: an update. *Acta crystallographica. Section D, Structural biology* **73**, 710-728

Table 1. Stability and Rap1A-Dependent Activation of PLCε Variants

PLCε variant	T_m ° C (n)	Basal specific activity (nmol IP_3/min/nmol PLCε variant) (n)	Fold Activation by $Rap1A^{G12V}$ (n)	EC_{50} for $Rap1A^{G12V}$ (n)
PH-COOH*	51.3 ± 0.72 (6)	360 ± 120 (9)	3.0 (4)	0.38 ± 0.3 (3)
EF3-COOH	51.7 ± 0.12 (4)	450 ± 50 (3)	N/A (3)	0.46 ± 0.03 (5)
PH-C2*	48.3 ± 1.00 (4)[a]	80 ± 20 (5)[a]	N/A (2)	1.6 ± 1.0[c] (3)
PH-COOH K2150A	50.5 ± 0.86 (3)	160 ± 30 (4)[b]	1.8 (2)	0.49 ± 0.1 (3)
PH-COOH K2152A	49.6 ± 0.79 (3)	240 ± 20 (3)	0.9 (3)	0.45 ± 0.1 (3)
PH-COOH Y2155A	49.8 ± 1.06 (3)	250 ± 40 (5)	1.4 (3)	0.29 ± 0.1 (3)
PH-COOH L2158A	51.2 ± 0.39 (3)	270 ± 100 (3)	1.0 (3)	0.44 ± 0.1 (3)
PH-COOH L2192A	51.5 ± 0.71 (3)	270 ± 50 (3)	1.3 (3)	0.40 ± 0.4 (3)
PH-COOH F2198A	51.5 ± 0.45 (3)	280 ± 100 (3)	1.2 (3)	0.39 ± 0.2 (3)

* T_m and specific activity for these variants were previously reported, and are included here for comparison (23).
[#]Maximum specific activities were measured at a single time point.
Results are based on one-way ANOVA followed by Dunnett's multiple comparisons test vs. PLCe PH-COOH. Error bars represent SD.
[a] ****$p \leq 0.0002$, [b] ** $p \leq 0.0028$, [c] * $p \leq 0.0163$.

Table 2. SAXS parameters of PLCε PH-COOH and EF3-COOH in complex with Rap1A^{G12V}

	PH-COOH[1]	Rap1A^{G12V}–PH-COOH	EF3-COOH	Rap1A^{G12V}–EF3-COOH
Guinier analysis				
I(0) (Arb.)	64.92 ± 0.21	1.66 ± 0.003	78.10 ± 0.43	26.96 ± 0.50
R_g (Å)	42.7 ± 0.17	42.4 ± 0.12	41.9 ± 0.43	36.8 ± 0.50
q min (Å^{-1})	0.0174	0.0043	0.0084	0.0094
q range (Å^{-1})	0.0174 - 0.0314	0.0043 - 0.0306	0.0084 - 0.0309	0.0094 - 0.352
P(r) analysis				
I(0) (Arb.)	65.96 ± 0.21	1.67 ± 0.03	79.43 ± 0.63	27.81 ± 0.21
R_g (Å)	44.79 ± 0.19	43.70 ± 0.16	44.48 ± 0.61	39.47 ± 0.43
D_{max} (Å)	162	165	175	145
Porod volume (Å^{-3})	191,000	237,000	179,000	178,000
q range (Å^{-1})	0.0174 - 0.308	0.0042 - 0.350	0.0087 – 0.387	0.0052 – 0.366

[1]The data for the PLCε PH-COOH variant was previously published, and is included for comparison (23).

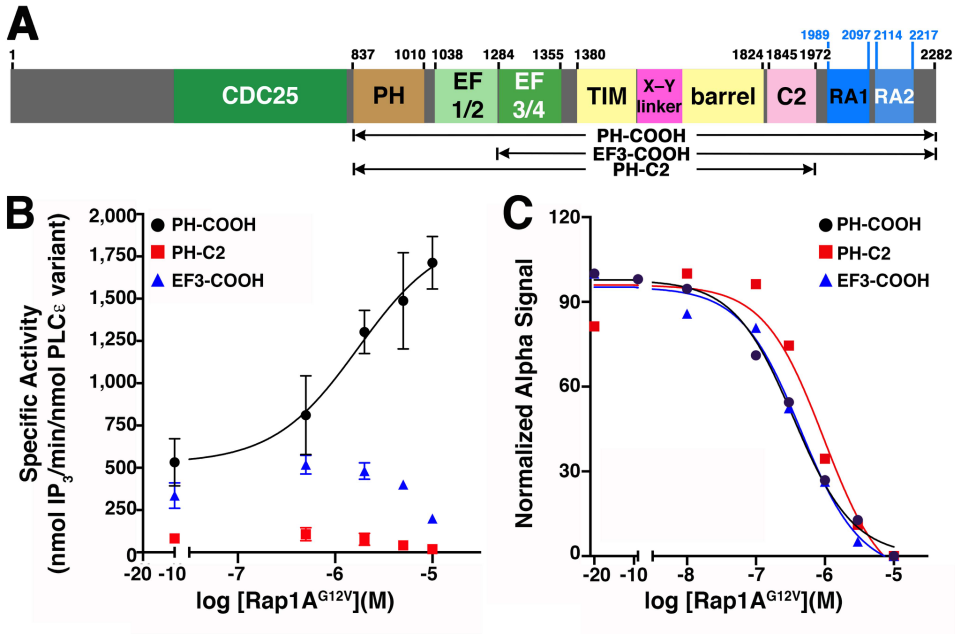

Figure 1. Multiple domains in PLCε are required for Rap1A^{G12V}-dependent activation. (A) Domain diagram of rat PLCε. Numbers above the diagram correspond to the domain boundaries most relevant to this work, with the variants under study shown below. (B) PLCε PH-COOH (black circles) is activated by Rap1A^{G12V} in a concentration-dependent manner. In contrast, PH-C2 (red squares) and EF3-COOH (blue triangles) are not activated at all concentrations of Rap1A^{G12V} tested. Data represents at least two independent experiments performed in duplicate. Error bars represent SD. (C) An AlphaLISA competition binding assay was used to measure the affinity between Rap1A^{G12V} and the PLCε domain deletion variants. PH-COOH (black circles) and EF3-COOH (blue triangles) bind Rap1A^{G12V} with comparable affinity, while PH-C2 (red squares) binds with ~4-fold weaker affinity. Representative curves are shown for the AlphaLISA binding assay.

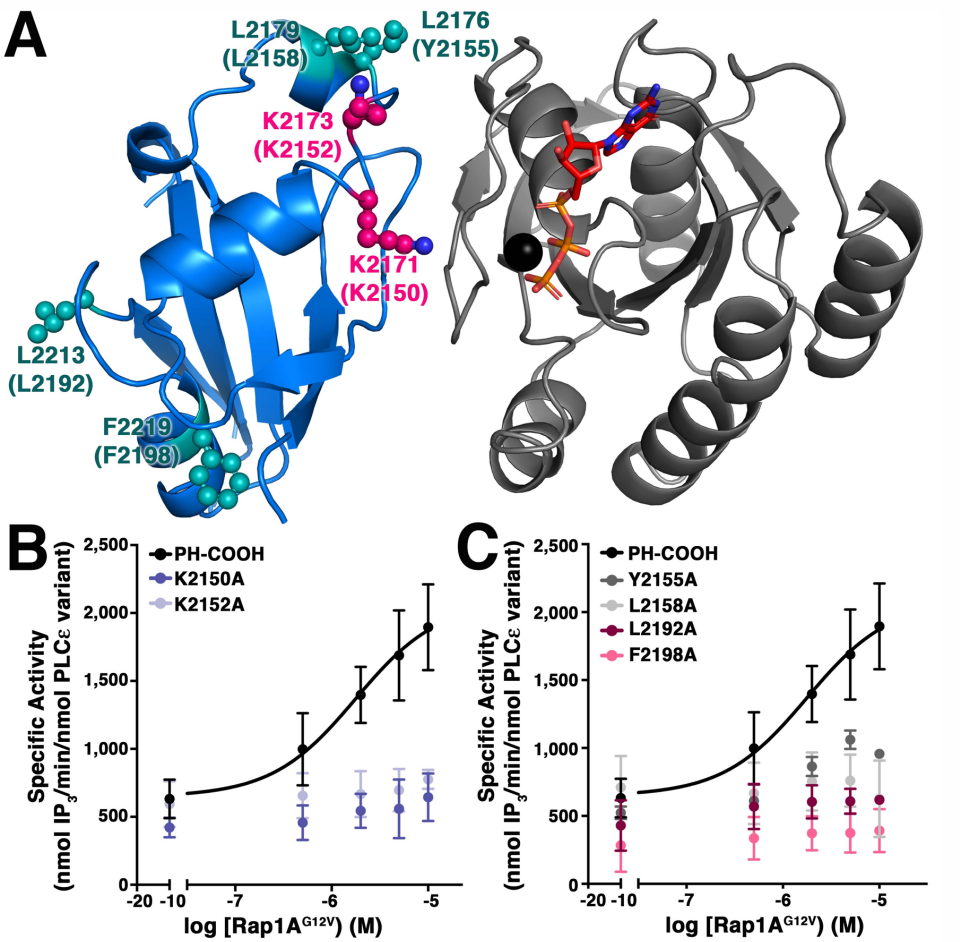

Figure 2. Hydrophobic residues on the surface of the RA2 domain are critical for activation. (A) The structure of H-Ras (gray) bound to the RA2 domain (marine, PDB ID 2C5L (12)) reveals conserved, hydrophobic residues (teal spheres) involved in crystal lattice contacts. K2171 and K2173 (hot pink spheres) were previously reported to be required for Rap1A-dependent activation. *R. norvegicus* residues are in parentheses. GTP is shown in orange sticks, and Mg^{2+} as a black sphere. (B) Mutation of the K2150 or K2152 to alanine eliminates activation by $Rap1A^{G12V}$ *in vitro*, as does (C) mutation of the conserved hydrophobic residues distant from the Rap1A binding surface.

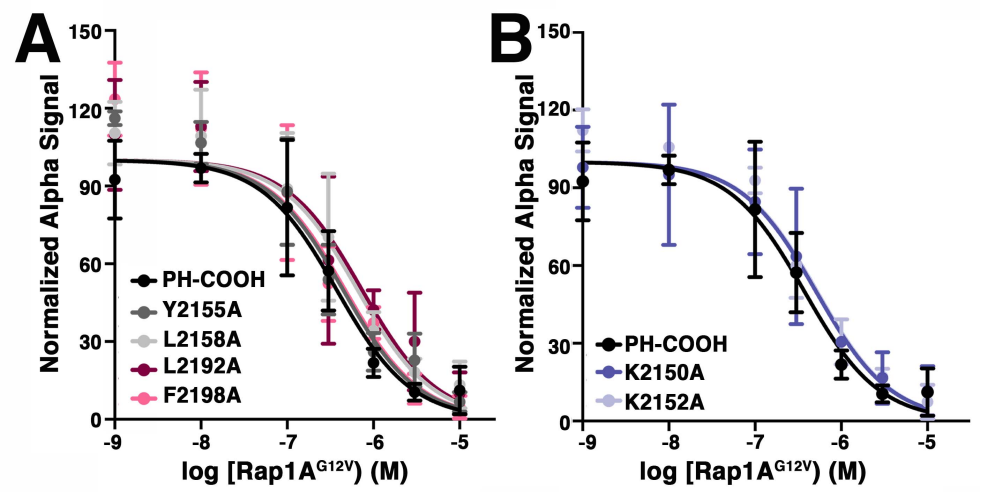

Figure 3. Mutation of conserved residues on the RA2 surface does not alter Rap1A^{G12V} binding. Mutation of (A) the conserved, hydrophobic surface residues or (B) lysines 2150 or 2152 to alanine has no impact on the binding affinity for Rap1A^{G12V}. Binding of PH-COOH to Rap1A^{G12V}, shown in Fig.1, is included for reference.

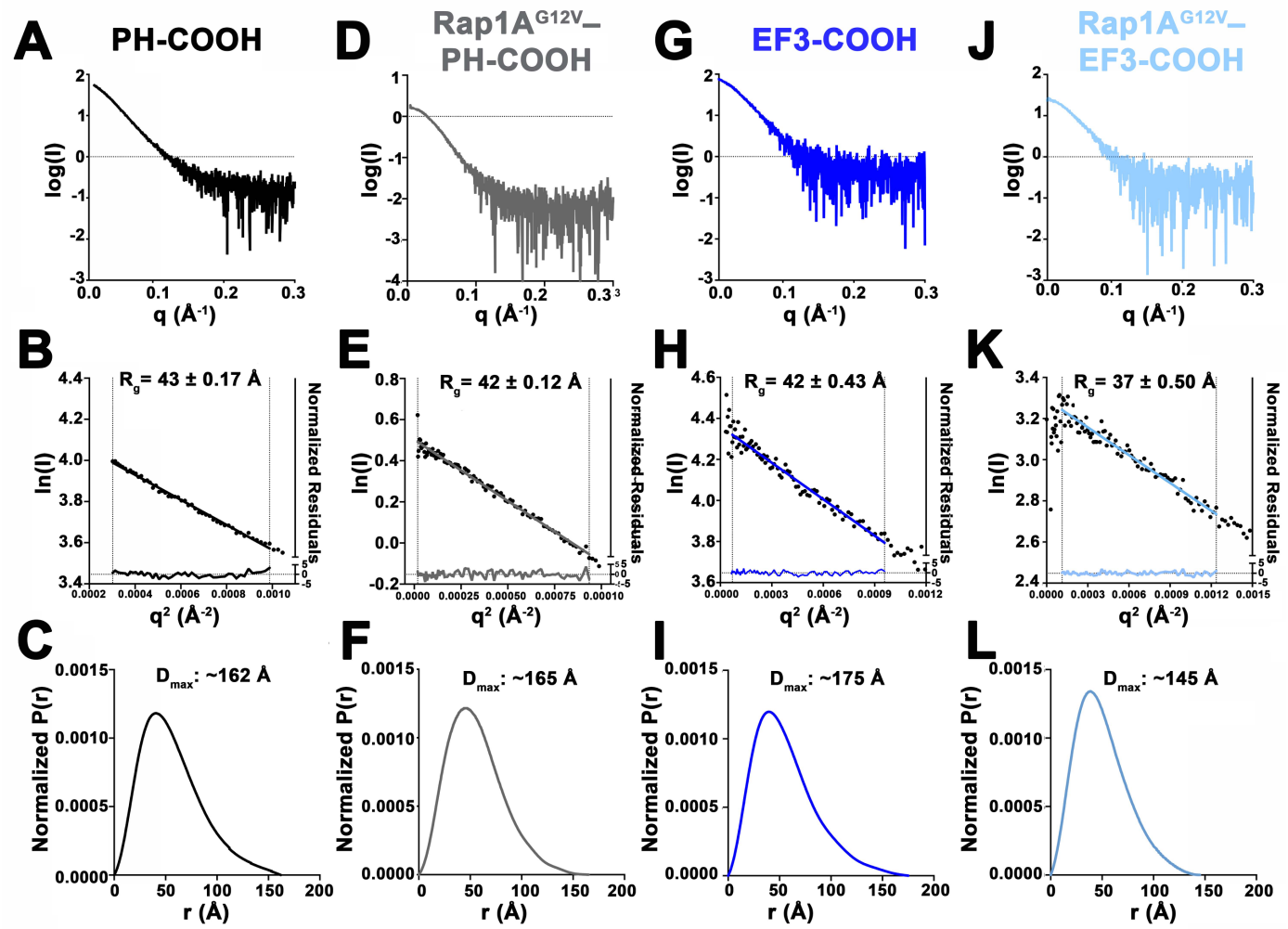

Figure 4. Rap1A^{G12V} binding to PLCε PH-COOH or EF3-COOH stabilizes different conformational states. The (A) scattering profile for PLCε PH-COOH and (B) Guinier plot demonstrate the variant is monomeric and monodisperse in solution. The (C) pair-distance distribution function is consistent with a largely globular protein with some extended features. The (D) scattering profile and (E) Guinier plot for the Rap1A^{G12V}–PH-COOH complex is also consistent with a monodisperse complex. The (F) pair-distance distribution function shows a more compact structure upon the binding of Rap1A^{G12V}. PLCε EF3-COOH is similar to PH-COOH in solution, as evidenced by its (G) scattering profile, (H) Guinier plot, and (I) pair-distance distribution function. The Rap1A^{G12V}–EF3-COOH complex does not have elevated lipase activity but is still monodisperse in solution as shown in (J) the scattering profile and (K) Guinier plot. However, the (L) shape of the pair-distance distribution function reveals the complex is more globular than EF3-COOH alone, and more compact, as evidenced by the smaller D_{max}. The data for the PLCε PH-COOH variant is included for comparison (23).

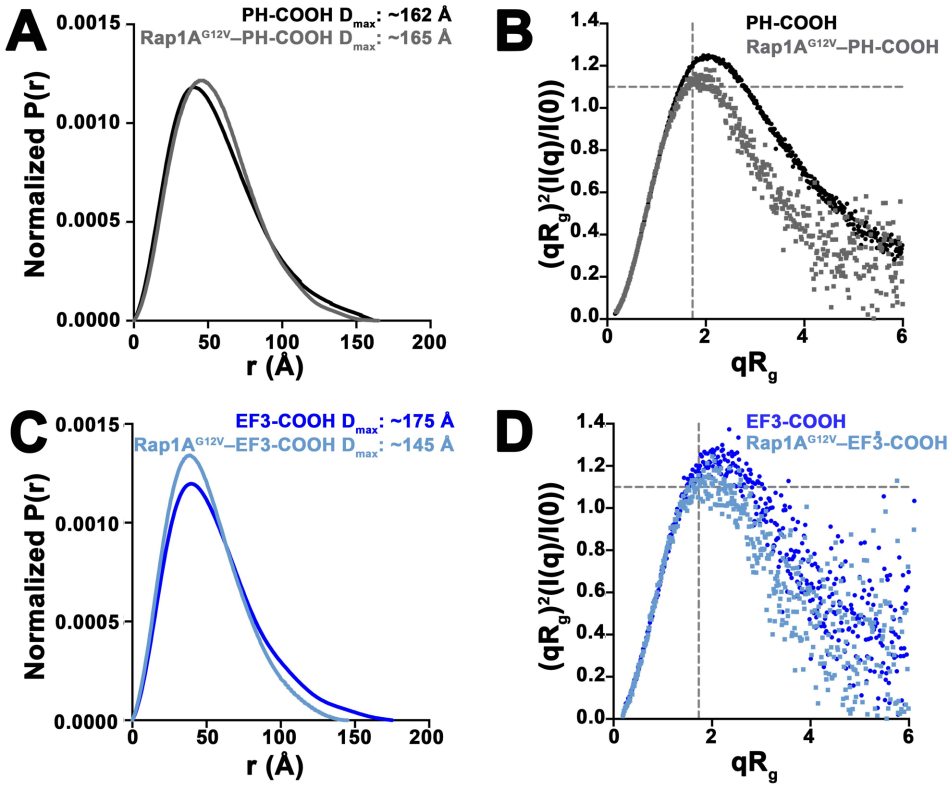

Figure 5. Normalized pair-distance and dimensionless Kratky plots for PLCε variants alone and in complex with Rap1A^{G12V}. (A) The normalized P(r) functions for PH-COOH and Rap1A^{G12V}–PH-COOH are similar with D_{max} values of ~162 Å and ~165 Å, respectively. (B) Comparison of PH-COOH (black circles) and Rap1A^{G12V}–PH-COOH (gray squares) show the complex is more compact and globular than PH-COOH alone, as evidenced by the more bell-shaped curve. (C) The normalized P(r) functions for EF3-COOH and Rap1A^{G12V}–EF3-COOH reveal binding of Rap1A^{G12V} induces substantial conformational changes that lead to a more compact structure. This is further supported by the ~30 Å decrease in D_{max} for the Rap1A^{G12V}–EF3-COOH complex. (D) Comparison of EF3-COOH (blue circles) and Rap1A^{G12V}–EF3-COOH (light blue squares). Rap1A^{G12V} binding induces conformational changes that result in a more compact and globular solution structure.

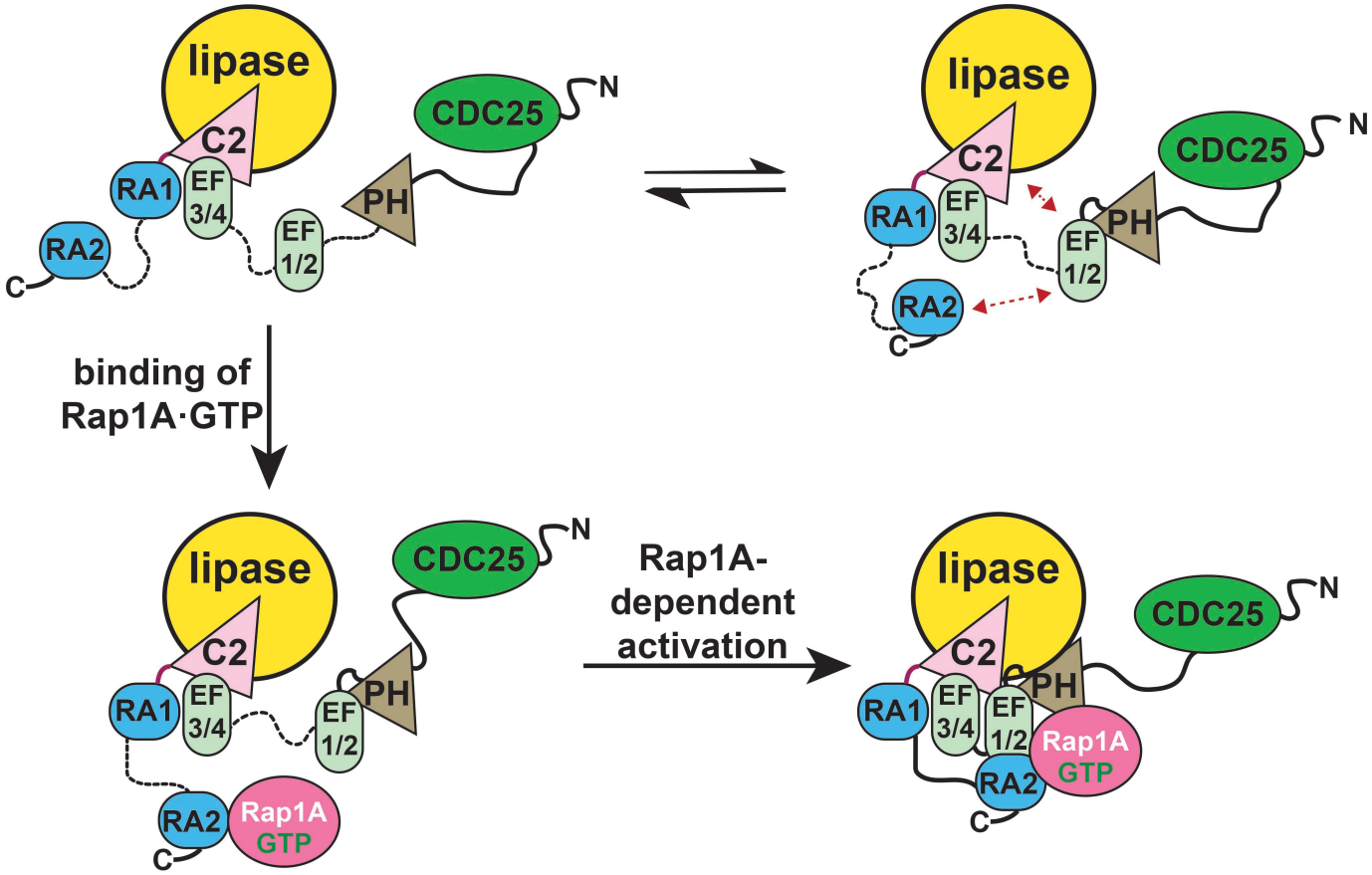

Figure 6. A model for activation of PLCε by Rap1A. (Top) PLCε exists in multiple conformational states in solution. The PH domain, EF1/2, and RA2 domains are flexibly connected to the rest of the enzyme, as indicated by the dashed black lines, and interact transiently with one another under basal conditions (23). (Bottom left) Activated Rap1A binds to its high affinity binding site on the PLCε RA2 domain. However, this interaction is insufficient on its own to activate lipase activity. (Bottom right) The Rap1A–RA2 complex also interacts with a site on the PLCε core, potentially formed by the PH domain and EF hands, which mediate Rap1A-dependent activation.